



Decentralised Droopless Control of Islanded Radial AC Microgrids Without Explicit Communication

DMITRY MILLER¹, GALINA MIRZAEVA ¹ (Senior Member, IEEE),
CHRISTOPHER DAVID TOWNSEND ² (Member, IEEE), AND GRAHAM C. GOODWIN¹ (Fellow, IEEE)

¹School of Engineering, The University of Newcastle, Callaghan, NSW 2308, Australia

²School of Engineering, University of Western Australia, Perth, WA 6009, Australia

CORRESPONDING AUTHOR: GALINA MIRZAEVA (e-mail: galina.mirzaeva@newcastle.edu.au)

This work was supported in part by the Australian Government through the Australian Research Council's Discovery Projects funding scheme under Grant DP190103307.

ABSTRACT A microgrid is a proven effective way to integrate renewable resources. This study presents an innovative control concept for decentralized AC microgrids, which is based on the architectural advantage of a radial microgrid structure. Under the proposed concept, power sharing between the distributed sources is achieved without droop control. Thus the need for a secondary control level is eliminated. Moreover, the use of explicit communication is replaced in the paper by a novel coordination mechanism based on the locally measured currents. The paper shows that, with a special design of the current control of grid-feeding converters, the proposed microgrid automatically provides equitable sharing of the load demand amongst the distributed generators (DGs). Moreover, the dynamic responses of the DGs are identical and decoupled from one another. It is further shown that the proposed AC microgrid is stable in the presence of any type of load. The findings of the paper are validated by simulations and laboratory experiments.

INDEX TERMS Microgrids, decentralized control, DC-AC power converters, distributed power generation.

I. INTRODUCTION

Traditional power systems worldwide are being complemented and/or superseded by Distributed Generators (DG) from renewable energy sources connected to grid via intelligent power converters [1], [2]. These converters can be broadly classified into grid feeding (or current controlled); grid forming (or voltage controlled); and grid supporting converters that can perform either role [3]. A current controlled converter (CCC) injects the requested amount of current, while a voltage controlled converter (VCC) establishes and regulates voltage under autonomous, or islanded, operation [3].

DG power converters, together with local loads, are typically organised into microgrids that can operate in grid-connected or islanded mode [4]. Depending on the type of common bus, microgrids can be DC or AC. Principles proposed in this paper equally apply to DC or AC microgrids.

The primarily focus of this paper is AC microgrid under islanded operation.

Microgrid control strategies are commonly based on a hierarchical structure [2]. The fastest control level is the primary control, which is responsible for sharing active and reactive power demand between DGs. Secondary control provides voltage/frequency restoration and other power quality functions. Tertiary control regulates power exchange of a microgrid with the main grid [5], [6]. The focus of the current paper is power sharing (primary) control of a microgrid in islanded mode, i.e. disconnected from the grid.

While centralized control is a common approach at the tertiary and secondary control levels [7], centralized power sharing control of islanded microgrids has found limited application, due to its dependence on high bandwidth telecommunication [8]. Decentralized droop control schemes are usually preferred at the primary control level [9], [10]. A

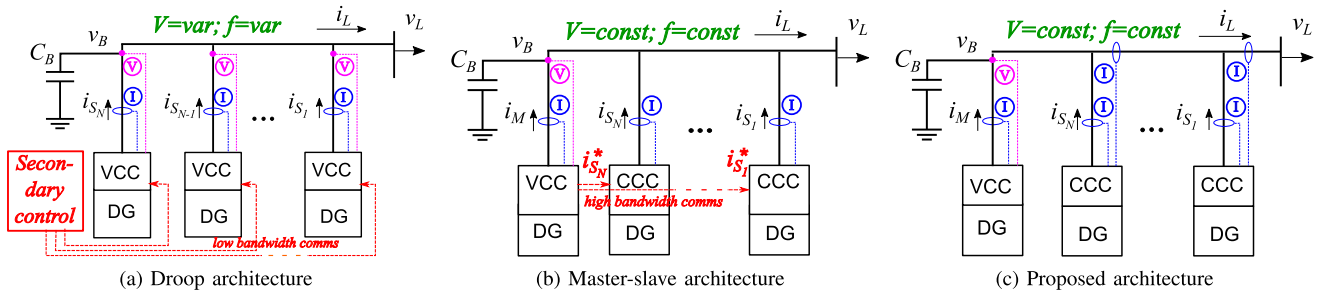


FIGURE 1. Control, communication and measurement under three microgrid architectures. (a) Droop architecture (b) Master-slave architecture (c) Proposed architecture.

droop control scheme is illustrated in Fig. 1(a). It involves parallel operation of VCCs whose real and reactive power outputs depend on voltage and frequency in a droop fashion [11].

To perform primary control, each VCC only requires information of voltage and current at the point of common coupling without communication links between individual inverters [12]. However, variations of the AC bus frequency and voltage by droop control require their restoration to the nominal values. This necessitates the use of the secondary control level that communicates global information to individual VCCs via lower bandwidth communication links, as shown in Fig. 1(a). In addition to the AC bus frequency and voltage, such global information may also include the required compensation of harmonics and unbalance of the load current [13], [14].

Various issues around decentralized microgrid operation have been addressed in the literature. Thus, undesirable coupling between VCCs can be mitigated by virtual impedances [15], [16] and other compensators [17]. Communication delays in passing global information to individual VCCs are addressed by using robust controllers [18], [19] or faster secondary level communication [20], [21]. A large body of the published work is dedicated to stability improvement of droop-controlled microgrids, particularly, in the context of constant power loads.

A constant power load (CPL) is the most challenging load type for grid stability, due to its negative differential impedance effect [22]. Small scale islanded AC and DC microgrids are particularly vulnerable to CPL. At the same time, a growing proportion of modern loads are connected to supply via power adaptors, thus exhibiting the CPL behaviour. Stabilisation strategies for microgrids with CPL include parameter optimization [23], special compensators [24] and other techniques [22].

Many of the issues around the operation of droop control can be attributed to its inherent competitive nature. That is, in the process of power sharing, multiple VCCs attempt to control the same characteristics (voltage and frequency) of the same AC bus. Such a competition is avoided in Master-Slave microgrid control where different DG power converters are assigned different control objectives, as illustrated in Fig. 1(b).

The Master (VCC) in Fig. 1(b) regulates the AC bus voltage and frequency around nominal values. Each Slave (CCC) controls only its own current, based on a reference received from the Master [25]. The reference, typically sent via high bandwidth communication, may include fundamental component, as well as harmonic and unbalance compensation [26]. Thus the need for the secondary control level is eliminated. The resulting control structure is simple, stable and robust.

Master-Slave architecture and its extensions have inspired many researchers. For example, in [25], [27], groups of power converters with a single Master and multiple Slaves are used as building blocks for larger microgrids. In such cases, Master VCCs can be synchronised via droop control [25] or communication [27]. Communication burden on Master VCC and vulnerability of microgrid due to a single point of failure are addressed by introducing virtual Masters in multi-agent systems with distributed communication [28]. Various combinations of Master-Slave and droop control, and the associated trade-offs, are explored in [18], [29].

This paper contributes to this ongoing discussion by proposing a novel principle of communication between the DG power converters, without utilizing droop or explicit communication links. The proposed principle explores the architectural advantages of the radial microgrid depicted in Fig. 1(c). All loads in this microgrid are connected at one end - at point v_L . One or more DGs associated with energy storage are connected, via VCCs, at the opposite end - at point v_B . The majority of DGs are connected to the microgrid bus, along its length, via CCCs.

The above architectural requirements can be easily satisfied in small size microgrids. By stretching the DG connectors over longer and non-equal distances, the desired connection can be achieved even in larger microgrids. Arrays of solar or wind DGs, microgrids for remote communities, residential microgrids with shared battery storage, industrial sites with distributed generation, on-board power systems for ships and aircrafts are amongst many practical scenarios, where the described architecture is suitable. Additionally, by using principles discussed in [25], [27], small microgrids with the proposed control can serve as building blocks for larger systems.

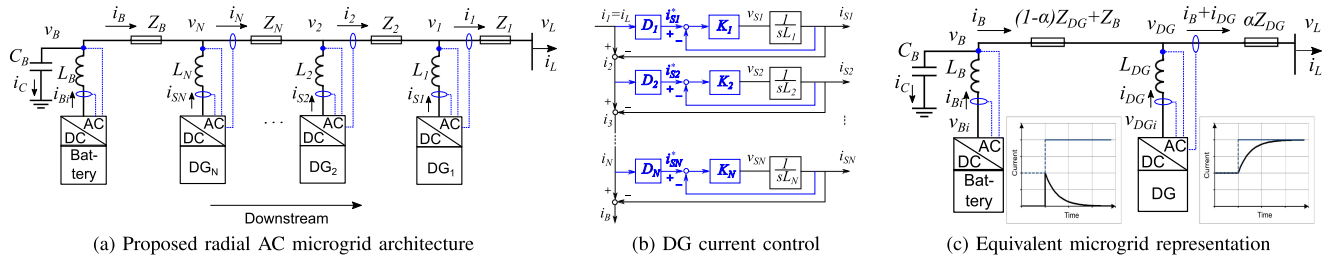


FIGURE 2. Proposed AC microgrid architecture, its control, and equivalent representation. (a) Proposed radial AC microgrid architecture (b) DG current control (c) Equivalent microgrid representation.

A major novel aspect of the proposed microgrid is its power sharing mechanism. Compared to droop (Fig. 1(a)) and Master-Slave (Fig. 1(b)) schemes, in the proposed scheme shown in Fig. 1(c) there is no secondary control and no explicit communication across the microgrid. In fact, at the control level, the DGs in Fig. 1(c) appear disconnected. An implicit communication is established based on an extra measurement, by each DG, of its local downstream current. The proposed scheme combines simplicity and inherent stability, as in Master-Slave control, with the advantage of decentralised control, as with droop. Due to independence from telecommunication, the proposed scheme enhances microgrid security and resilience.

The paper is structured as follows.

Section II describes the proposed architecture and control concept. Section III discusses implementation and stability aspects, supported by simulations. Section IV provides experimental validation. Section V discusses extensions. Section VI provides conclusions.

II. IMPLICIT COMMUNICATION MECHANISM

Fig. 2(a) illustrates a radial AC microgrid with N DGs and a Battery Storage System (BSS), connected to common AC bus via power converters. Connection to the main grid can be made at the battery side, at the point v_B . The microgrid loads are connected at the point v_L . All DG inverters are CCC.

Each DG_j (where $j = 1, \dots, N$) is provided with local measurements of: downstream current i_j (immediately to the right from the connection point); and its own output current i_{Sj} . The proposed implicit communication mechanism includes:

- a special way of obtaining current references for CCCs, that is, the current reference for each CCC is formed as a given share D_j of its measured downstream current: $i_{Sj}^* = D_j i_j$;
- a special way of setting current control gains for CCCs, that is, the current control gain of each CCC is given by (3) and depends on the CCC position relative to others. Identical DG inverters are not expected to have equal control gains.

These two features lead to an automatic coordination of the DG inverter responses to load changes, as described below. This section, for simplicity, operates with DC voltages and currents (implying dq -components of AC signals). In Section III, the proposed concept is fully adapted to AC microgrids.

A. DYNAMICS OF GRID FEEDING CONVERTERS (CCC)

Fig. 2(b) shows the proposed control scheme for DG inverters, where the flow of physical signals is shown in black, and the flow of data processing is shown in blue. Conceptually, each CCC can be represented by an integrator with closed loop current control around it. The current control gain is K_j , and the inductance associated with the integrator is L_j . Then the output current of each DG inverter is described by:

$$i_{Sj} = \frac{i_{Sj}^*}{1 + (L_j/K_j)s} = \frac{D_j i_j}{1 + (L_j/K_j)s} \quad (1)$$

where D_j is the share with respect to downstream current. If E_j is the share with respect to the total load current, then the difference between D_j and E_j can be seen by comparing

$$E_j = \frac{S_j}{\sum_{k=1}^N S_k} \quad \text{and} \quad D_j = \frac{S_j}{\sum_{k=j}^N S_k} \quad (2)$$

where S_j is the rating of the j -th DG inverter.

Note that $\sum_{j=1}^N E_j = 1$; $D_1 = E_1$; and $D_j \neq E_j$ for $j > 1$. The control gains K_j are set in such a way that all DGs have identical dynamics in response to a load step change. A detailed derivation can be found in [30], resulting in:

$$K_j = \frac{L_j}{L_1} K_1 \frac{E_j}{D_j} = \frac{L_j}{L_1} K_1 \sum_{k=j}^N S_k / \sum_{k=1}^N S_k \quad (3)$$

To illustrate, assume that 4 identical DGs carry equal shares in the total load current. This means that $E_j = 1/4$ ($j = 1, \dots, 4$). Then, according to (2), DG1 supplies $D_1 = 1/4$ of its downstream current; DG2 supplies $D_2 = 1/3$; DG3 supplies $D_3 = 1/2$; and DG4 (the leftmost DG in Fig. 2(a)) supplies $D_4 = 1$, or the entire downstream current that it measures. If the coupling inductances L_j are also equal then, according to (3), the control gains should be selected as: K_1 , $K_2 = \frac{3}{4}K_1$, $K_3 = \frac{1}{2}K_1$ and $K_4 = \frac{1}{4}K_1$.

It will be now shown that, by forming the DG current references from the downstream current as $D_j i_L$, and by selecting the DG control gains K_j according to (3), the following objectives are automatically achieved:

- DGs share the load current in proportion to their capacity;
- dynamic responses of individual DGs are identical, and the combined response is described by a first order system;
- current produced by each DG is decoupled from others.

For the rightmost inverter DG1 the gain is independently selected as K_1 . Its measured downstream current i_1 equals to the total load current i_L , and its reference equals to $D_1 i_L$. Therefore, the control of DG1 is independent of other DGs. Based on (1), the output current of DG1 is obtained as:

$$i_{S1} = i_L \frac{D_1}{1 + \frac{L_1}{K_1} s} = i_L \frac{E_1}{1 + \frac{L_1}{K_1} s} \quad (4)$$

Note that, according to (2), $D_1 = E_1$. For the next inverter DG2, the measured downstream current is the total load current i_L reduced by the amount i_{S1} . Substituting from (4) yields:

$$i_2 = i_L - i_{S1} = i_L \frac{1 - E_1 + \frac{L_1}{K_1} s}{1 + \frac{L_1}{K_1} s} \quad (5)$$

The output current from DG2 can be determined from (1), with the control gain $K_2 = \frac{L_2}{L_1} K_1 \frac{E_2}{D_2}$, according to (3). Then:

$$i_{S2} = i_2 \frac{D_2}{1 + \frac{L_2}{K_2} s} = i_2 \frac{D_2}{1 + \frac{L_1 D_2}{K_1 E_2} s} \quad (6)$$

Finally, expression (5) for i_2 is substituted into (6). The $1 - E_1$ term can be replaced by its value calculated as: $1 - E_1 = 1 - S_1 / \sum_{k=1}^N S_k = \sum_{k=2}^N S_k / \sum_{k=1}^N S_k = \frac{E_2}{D_2}$. This results in:

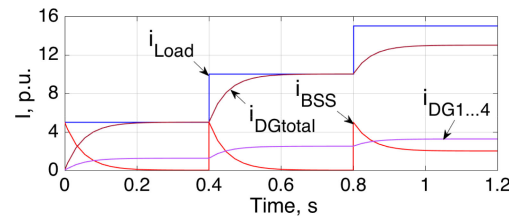
$$i_{S2} = i_L \frac{\frac{E_2}{D_2} \left(1 + \frac{L_1 D_2}{K_1 E_2} s\right)}{1 + \frac{L_1}{K_1} s} \frac{D_2}{1 + \frac{L_1 D_2}{K_1 E_2} s} = i_L \frac{E_2}{1 + \frac{L_1}{K_1} s} \quad (7)$$

Comparing the output currents from DG1 (4) and DG2 (7), it can be seen that the steady state shares of DG1 and DG2 in the total current are, respectively, E_1 and E_2 , as desired. Both currents (7) and (4) have first order dynamics with identical time constant given by $\tau = L_1 / K_1$.

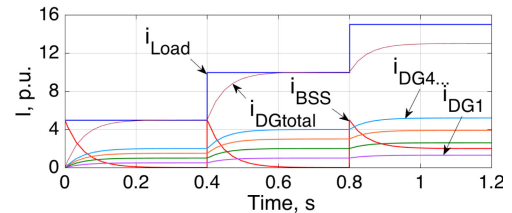
Furthermore, currents from DG1 and DG2 are independent of each other and only depend on the load current, despite that DG1 and DG2 appear coupled via the reference arrangement. However, as seen from (7), DG2 own dynamics become cancelled, and DG2 adopts the dynamics of DG1.

The same steps can be repeated for the next inverter. Each inverter in the chain replicates the dynamic response of its neighbour on the right. In the end, all inverters replicate the dynamic response of the rightmost, independently set, DG1 inverter. The combined output current from all DG inverters:

$$i_{DG} = \sum_{j=1}^N i_{Sj} = \sum_{j=1}^N E_j i_L \frac{1}{1 + s\tau} = i_L \frac{1}{1 + s\tau} \quad (8)$$



(a) Equal DG inverter currents



(b) Unequal DG inverter currents

FIGURE 3. Response to load step changes of the example microgrid. (a) Equal DG inverter currents (b) Unequal DG inverter currents.

The earlier described example with 4 DGs is illustrated by a conceptual (DC current) simulation in Fig. 3(a). Traces of all DG currents $i_{DG1} \dots i_{DG4}$ are coincident, as expected. In Fig. 3(b) the case is modified so as DGs have unequal ratings and carry 0.1; 0.2; 0.3; 0.4 of the total load current. The new gains, selected according to (3) are: K_1 ; $0.9K_1$; $0.7K_1$; $0.4K_1$, respectively. Traces of the DG currents are now different but their time constants are identical. The same currents, weighted by their respective ratings, are identical to those in Fig. 3(a).

B. DYNAMICS OF GRID FORMING CONVERTER (VCC)

The combined response of all DG inverters to the load change is described by a first order lag (8). Therefore, a step change in the load current demand cannot be instantly met by the DG inverters alone. However, in the derivation of the expression (8) it was assumed that the load current demand is immediately satisfied, so that $i_1 = i_L$.

This problem is resolved if the leftmost device in the system, which is the BSS inverter, operates as a fast responding current source. BSS shown in Fig. 2(a) may contain one or more battery units and is supported by the capacitor C_B . The BSS inverter works under closed loop voltage control (as VCC), keeping v_B around its set point value v_{PCC} . This control must be at least an order of magnitude faster than the DG current control. Under these conditions, in response to a load step change, BSS will supply the transient difference between the load current demand and the total DG current: $i_B = i_L - i_{DG}$.

If the combined DG power is sufficient to satisfy the load demand, then BSS only supplies the load transients. In situations when the combined DG power is not sufficient, BSS will also participate in the steady state current sharing. Taking this

into account, the BSS output current is described by:

$$i_B = i_L - i_{DG} = \begin{cases} i_L \frac{s\tau}{1+s\tau} & \text{if } i_{DGmax} \geq i_L \\ i_{DGmax} \frac{s\tau}{1+s\tau} + (i_L - i_{DGmax}) & \text{if } i_{DGmax} < i_L \end{cases} \quad (9)$$

In Fig. 3, after $t = 0.8s$ the total DG current capacity $i_{DGmax} = 13$ A is exceeded, and BSS automatically supplies the remaining 2 A in steady state, by virtue of its voltage control.

With the help of Fig. 2(a), voltage at the load connection point can be determined as:

$$v_L = v_{PCC} - Z_1(i_{S1} + \dots + i_{SN} + i_B) - Z_2(i_{S2} + \dots + i_{SN} + i_B) - \dots - Z_N(i_{SN} + i_B) - Z_B i_B \quad (10)$$

According to (8), currents i_{Sj} in (10) can be expressed as shares in the total DG current: $i_{Sj} = E_j i_{DG}$. The AC bus impedance between BSS and the load is denoted as $Z_{DG} = Z_1 + Z_2 + \dots + Z_N$, and coefficient α is introduced such that:

$$\alpha = \frac{Z_1 + Z_2(E_2 + \dots + E_N) + \dots + Z_N E_N}{Z_{DG}} \quad (11)$$

where $\alpha < 1$. Then expression (10) can be simply written as:

$$v_L = v_{PCC} - \alpha Z_{DG} i_{DG} - (Z_{DG} + Z_B) i_B \quad (12)$$

Previously, based on expression (8), all microgrid DG currents have been replaced by a single equivalent current i_{DG} . Now, based on expression (12), all microgrid bus impedances are replaced by two equivalent impedances: αZ_{DG} and $(Z_{DG} + Z_B)$. With these simplifications, the entire microgrid with any number of DGs and batteries, of equal or non-equal ratings, can be represented as a simple equivalent microgrid with only two sources: combined DG and BSS. Fig. 2(c) illustrates the equivalent microgrid circuit.

C. STABILITY OF THE PROPOSED MICROGRID FOR DIFFERENT LOAD TYPES

Expressions (8) and (9) for the microgrid currents correspond to the following time domain solutions:

$$i_{DG}(t) = i_L^o + (i_L^s - i_L^o) \left(1 - e^{-\frac{t}{\tau}}\right) \quad (13)$$

$$i_B(t) = \tau \frac{di_{DG}(t)}{dt} = (i_L^s - i_L^o) e^{-\frac{t}{\tau}} \quad (14)$$

where i_L^o and i_L^s are steady state load currents before and after a step change; and $\tau = L_1/K_1$. Assuming, for simplicity, resistive impedances of the microgrid connections ($Z_{DG} = R_{DG}$, $Z_B = R_B$), and substituting (13) and (14) into (12) results in the following load side voltage:

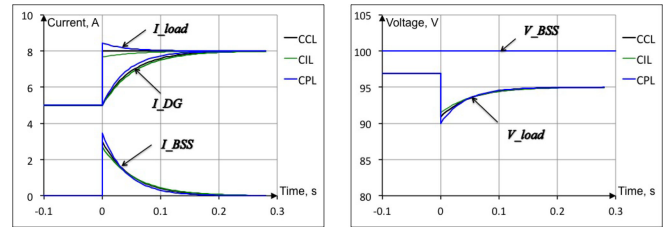
$$v_L(t) = v_{PCC} - \alpha R_{DG} i_L^s - R_{eq} (i_L^s - i_L^o) e^{-\frac{t}{\tau}} \quad (15)$$

where $R_{eq} = R_B + (1 - \alpha)R_{DG}$.

The stable first order dynamics, described by expressions (13)–(15), has been obtained assuming that the microgrid load behaves as a current source. This type of load is known in literature as constant current load (CCL), while a realistic load is typically a combination of constant impedance load (CIL) and constant power load (CPL) [23].

TABLE 1. Parameters for Different Load Types

	CIL	CPL
$i_L(i_{DG})$	$\frac{V_{PCC} + R_{eq} i_{DG}}{R_L + R_{DG} + R_B}$	$\frac{(V_{PCC} - \frac{R_{eq} i_{DG}}{f(P_L)})(1 - f(P_L))}{2(R_{DG} + R_B)}$
i_L^o	$\frac{V_{PCC}}{R_L^o + \alpha R_{DG}}$	$\frac{V_{PCC}(1 - f(P_L^o))}{2(R_{DG} + R_B) + R_{eq} \left(\frac{1}{f(P_L^o)} - 1\right)}$
i_L^s	$\frac{V_{PCC}}{R_L^s + \alpha R_{DG}}$	$\frac{V_{PCC}(1 - f(P_L^s))}{2(R_{DG} + R_B) + R_{eq} \left(\frac{1}{f(P_L^s)} - 1\right)}$
τ'	$\tau \frac{R_L^s + R_{DG} + R_B}{R_L^s + \alpha R_{DG}}$	$\tau \frac{2(R_B + R_{DG})}{2(R_B + R_{DG}) + R_{eq} \left(\frac{1}{f(P_L^s)} - 1\right)}$
		where $f(P_L) = \sqrt{1 - 4P_L(R_B + R_{DG})/V_{PCC}^2}$



(a) Theoretical currents compared (b) Theoretical voltages compared

FIGURE 4. Currents and voltages for CCL, CIL and CPL. (a) Theoretical currents compared (b) Theoretical voltages compared.

Results obtained for CCL can be easily extended to CIL and CPL. In all cases, the following fundamental equation applies:

$$i_L(t) = i_{DG}(t) + \tau \frac{di_{DG}(t)}{dt} \quad (16)$$

An equivalent form of the load voltage expression (12) is:

$$v_L = v_{PCC} - (R_B + R_{DG})i_L + R_{eq}i_{DG} \quad (17)$$

Expression (17) can be substituted into $i_L = \frac{v_L}{R_L}$ (CIL) or $i_L = \frac{P_L}{v_L}$ (CPL). Then i_L can be expressed in terms of i_{DG} and substituted into the fundamental (16), which can be solved for $i_{DG}(t)$. It was found that the resulting solutions for $i_{DG}(t)$ for CIL and CPL have the same form (13) as for CCL, except that i_L^o and i_L^s are expressed in terms of load resistance (R_L) or load power (P_L), before and after the change. Additionally, the new time constant τ' is slightly bigger than τ in CIL case and slightly smaller than τ in CPL case. Table 1 shows relevant expressions for CIL and CPL.

Knowing $i_{DG}(t)$, other microgrid quantities can be determined from (14), (16) and (17). Theoretical microgrid currents and voltages, obtained for CCL, CIL and CPL cases, are compared in Fig. 4(a) and (b). From this analysis it follows that, under the proposed control, the microgrid is not very sensitive to the load type, and is stable in all cases.

It is possible to even further improve the microgrid dynamics and make it completely insensitive to the load type. This can be achieved by dynamically adjusting the BSS voltage

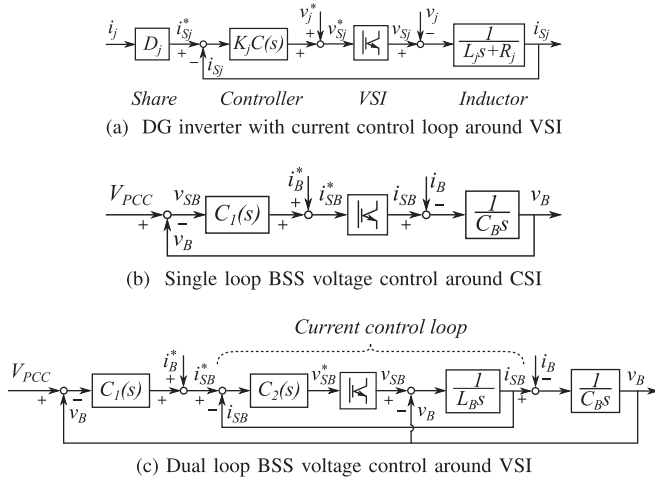


FIGURE 5. Implementation of DG and BSS inverter control. (a) DG inverter with current control loop around VSI (b) Single loop BSS voltage control around CSI (c) Dual loop BSS voltage control around VSI.

reference by a term dependent on the measured BSS current, as: $V_{PCC} + R_{eq}i_B$. Such an adjustment decouples i_L and i_{DG} by replacing expression (17) with

$$v_L = v_{PCC} - \alpha R_{DG}i_L \quad (18)$$

In CIL and CPL cases this means that, if the load impedance or load power undergo a step change, then the load current undergoes an immediate step change. This makes CCL, CIL or CPL appear to the microgrid as CCL.

III. IMPLEMENTATION ASPECTS AND SIMULATIONS

The proposed concept formulated in Section II in DC domain, can be easily adapted to AC domain. The following expressions describe voltages across the DG coupling inductor in rotating dq -frame [31]:

$$\begin{cases} v_{Sj}^d - v_j^d = R_j i_{Sj}^d + L_j \frac{di_{Sj}^d}{dt} - \omega L_j i_{Sj}^q \\ v_{Sj}^q - v_j^q = R_j i_{Sj}^q + L_j \frac{di_{Sj}^q}{dt} + \omega L_j i_{Sj}^d \end{cases} \quad (19)$$

where v_{Sj} and v_j are output voltage and voltage at the coupling point of the DG $_j$ inverter, respectively; i_{Sj} is the current supplied by the DG $_j$ inverter; L_j is inductance and R_j is resistance of the coupling inductor; and ω is the angular velocity of the rotating dq -frame.

A natural choice for implementation of DG inverters is a current controlled Voltage Source Inverter (VSI). Control diagram for inverter DG $_j$ is shown in Fig. 5(a) for one axis only (d or q). The dq -frame is aligned with the coupling voltage: $v_j^d = v_j$, $v_j^q = 0$. Current references i_{Sj}^{d*} , i_{Sj}^{q*} are formed from the measured downstream current i_j . Controller $C(s)$ is a PI controller with gain 1, and K_j is chosen as per (3). Voltage v_j^* , fedforward to the VSI reference, includes the cross-coupling compensation [32]: $v_j^{d*} = v_j^d - \omega L_j i_{DGj}^q$; $v_j^{q*} = \omega L_j i_{DGj}^d$.

If the time constant of the PI controller matches L_j/R_j then the closed loop transfer function from the reference i_{Sj}^*

TABLE 2. Microgrid Parameters Used in the Studies

Parameter	Simulation value	Experimental value	Units
V_{PCC}	100	50	V
R_B	1	0.7	Ohm
R_{DG}	0.5	0.25	Ohm
I_{load}	5-15	1-2	A
DG L_{filter}	50	53	mH
BSS L_{filter}	10	53	mH
BSS C_{filter}	100	22	μ F
DG, BSS V_{DC}	580	110	V
DG, BSS f_{sw}	10	5	kHz
BSS $C_2(s)\tau$	2	1	ms
BSS $C_1(s)\tau$	20	10	ms
DG $C(s)\tau$	50	80	ms
CPL $C(s)\tau$	1	0.7	ms

to the actual current i_{Sj} is given by $1/(1 + sL_j/K_j)$, which is identical to (1). This leads to the combined DG current dynamics as per expression (8).

Since the functionality of the BSS inverter is dual to that of the DG, a voltage controlled current source inverter (CSI) is an appropriate choice. It can be implemented directly, as shown in Fig. 5(b), or indirectly, by a dual loop control around VSI, as shown in Fig. 5(c). The second option has been chosen in this study. It is important that the BSS inner current control loop is at least 10 times faster than the outer voltage control loop, and that the BSS voltage control loop is at least 10 times faster than the DG current control loop [33].

To validate the proposed AC microgrid architecture and control, detailed simulations were performed in Matlab/Simulink environment. The simulated AC microgrid followed the architecture shown in Fig. 2(a) and included four DGs and one BSS. Control of each DG inverter was implemented according to Fig. 5(a) and control of the BSS inverter - according to Fig. 5(c). Parameters used in the simulations are shown in Table 2.

The AC microgrid simulation plots are shown in Fig. 6. They follow the same logic as the conceptual (DC) plots in Fig. 3. Fig. 6(a) illustrates the d -axis currents corresponding to equal current sharing between DGs, and Fig. 6(c) shows the same currents for unequal current sharing, namely, as 10%, 20%, 30% and 40%. In both cases, the total current capacity of all DG inverters is 13 A and the load is purely resistive.

The load current undergoes three steps: from 0 to 5 A at $t = 0$ s, from 5 A to 10 A at $t = 0.4$ s, and from 10 A to 15 A at $t = 0.8$ s. Dynamics of the four DGs are identical in Fig. 6(a), and have the same time constant in Fig. 6(c), as expected. The BSS inverter supplies transients and carries no steady state current, until $t = 0.8$ s. After that, according to (9), the BSS inverter supplies the remaining 2 A in steady state.

Further, Fig. 6(d) shows the load side voltage, in both dq - and stationary frames. With the q -axis voltage being trivial, the d -axis component corresponds to the ‘‘envelope’’ of the AC waveform. Additionally, Fig. 6(b) shows q -axis currents for the case of equal current sharing (note $10\times$ y-axis scaling). Very small values of q -axis currents confirm effective decoupling.

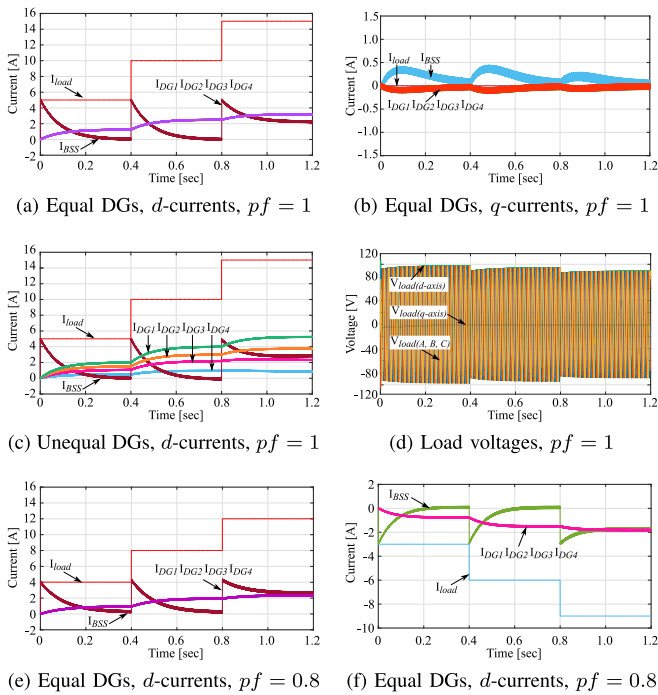


FIGURE 6. DG current sharing under the proposed scheme. (a) Equal DGs, d -currents, $pf = 1$ (b) Equal DGs, q -currents, $pf = 1$ (c) Unequal DGs, d -currents, $pf = 1$ (d) Load voltages, $pf = 1$ (e) Equal DGs, d -currents, $pf = 0.8$ (f) Equal DGs, d -currents, $pf = 0.8$.

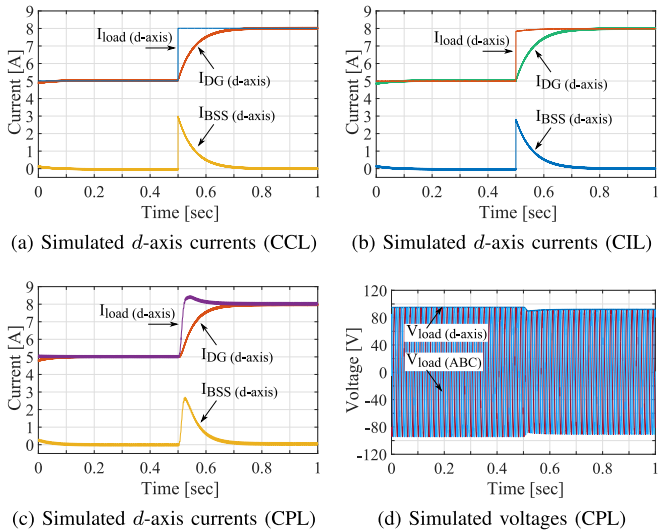


FIGURE 7. Microgrid simulations under different loads types. (a) Simulated d -axis currents (CCL) (b) Simulated d -axis currents (CIL) (c) Simulated d -axis currents (CPL) (d) Simulated voltages (CPL).

Finally, Fig. 6(e) and (f) illustrate d - and q - axis microgrid currents when supplying an inductive AC load with power factor 0.8 (lag). Each current component is controlled practically independently, and the cross-coupling effect is unnoticeable.

Fig. 7 illustrates the AC microgrid response to a load step change for CCL, CIL and CPL. The d -axis currents shown

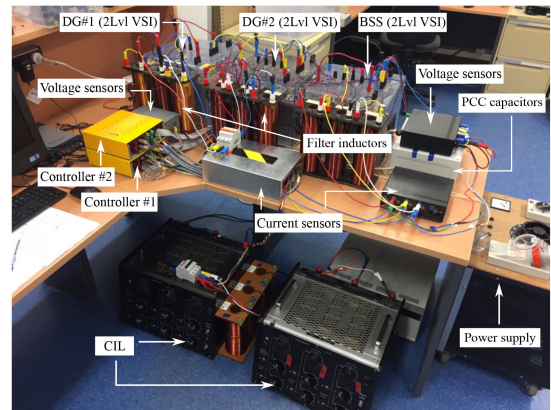


FIGURE 8. Experimental setup (CIL configuration).

in Fig. 7(a), (b), and (c) closely follow the conceptual plots of Fig. 4(a). Load voltages are illustrated in Fig. 7(d) for the CPL case only.

IV. EXPERIMENTAL VALIDATION

To validate the proposed concept, an experimental AC microgrid system was developed as shown in Fig 8. The first set of experiments was designed to prove the capability of the proposed microgrid to share the load current, in a desired way, based on the local measurements only. The experimental AC microgrid in this case included 2 DG inverters and 1 BSS inverter feeding a resistive load. Each inverter was independently controlled by a 32-bit TMS320F28335 DSP. Parameters of the microgrid components are shown in Table II, column 3. Experiments plots are shown in Fig. 9.

The DG inverters were current controlled in dq -frame, as per Fig. 5(a). The BSS inverter operated under a cascaded voltage control in dq -frame, corresponding to Fig. 5(c). The AC bus voltage 50V(rms) and frequency 50 Hz were established by the BSS inverter and remained unchanged. The DG inverters were synchronised to the microgrid frequency by PLL on voltages measured at their connection points. Currents references were obtained from the measured downstream currents.

In Fig. 9, at time 0.6 s the load current undergoes a step change from 1.2 A to 2.4 A. Fig. 9(a) illustrates the case when the DG inverters have equal capacity and share the load current in proportion 50:50. In Fig. 9(c) corresponds to unequal sharing in proportion 70:30. In both cases the step change of the load current is initially supplied by BSS and is then shared between the DGs in the desired proportion. Fig. 9(b) shows that the q -axis currents remain practically zero, which proves effective decoupling. The load voltage illustrated in Fig. 9(d), after a small dip, recovers to practically the same value.

The second set of experiments validated stability of the proposed AC microgrid with respect to different load types. Experimental plots are shown in Fig. 10. The CIL, CCL and CPL loads were represented, respectively, by: a resistive load; an active AC/DC converter with controlled AC current;

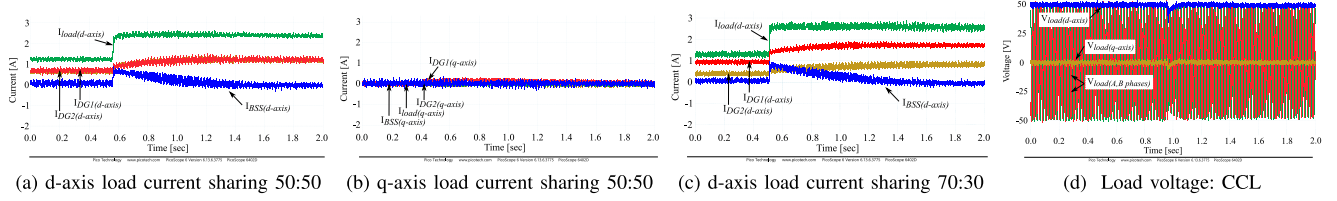


FIGURE 9. Different DG load power sharing in experimental microgrid. (a) d-axis load current sharing 50:50 (b) q-axis load current sharing 50:50 (c) d-axis load current sharing 70:30 (d) Load voltage: CCL.

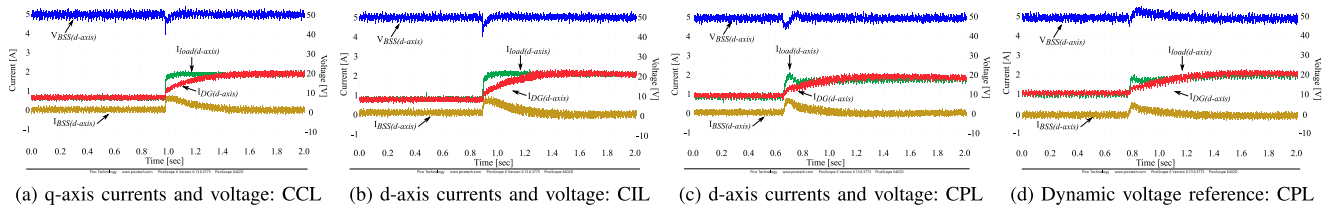


FIGURE 10. Experimental microgrid under different load types. (a) q-axis currents and voltage: CCL (b) d-axis currents and voltage: CIL (c) d-axis currents and voltage: CPL (d) Dynamic voltage reference: CPL.

and an active AC/DC converter with controlled DC power. The current dynamics observed in the experimental plots of Fig. 10(a), (b), and (c) are very similar to the corresponding simulation plots of Fig. 7(b), (c), and (d). In all cases, microgrid exhibited stable behaviour, and the DG and the BSS currents followed the first order dynamics, as expected. Additionally, the dynamic voltage reference variation with the CPL load, discussed in Section II-C, is illustrated in Fig. 10(d). This strategy reduced the overshoot in the load current and regulated the BSS voltage closer to a constant value.

It should be noted that experimental results presented in this section were obtained in the presence of small unbalance of the load and coupling impedances between the three phases. Such an unbalance caused some ripple in the dq quantities but did not impede the microgrid performance in general. This is due to its inherent capacity to share not only the fundamental, but also the harmonic and unbalance current components.

V. FLEXIBILITY AND FAULT TOLERANCE

Under the proposed architecture, the settings (D_j, K_j) of each individual DG inverter depend on knowledge of its share with respect the total current capacity $\sum_{j=1}^N S_j$, i.e. on the global information. It is possible, however, that energy available to some of the DG inverters may change over time, which affects the total current capacity. One such example is a change of photovoltaic energy due to a cloud, which may affect individual PV cells differently. Another example is a failure of one of the DGs due to a fault.

Under changed conditions, DG inverters should be able to adjust their shares and gains. If such a functionality is desirable, then all microgrid architectures shown in Fig. 1 require modifications. The standard approach for Master-Slave or droop control schemes is the addition of a low bandwidth

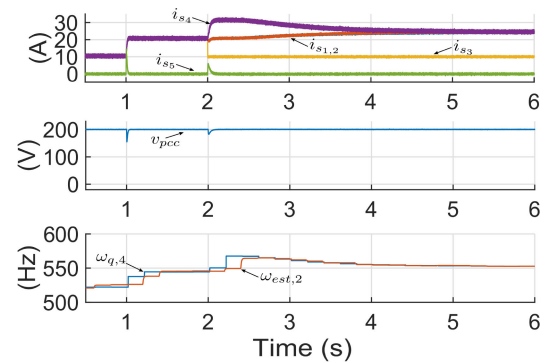


FIGURE 11. DG current adjustment by using PLC (simulation).

telecommunication channel from Slaves to Master, or from DG to secondary control, respectively.

The same approach can be applied to the proposed architecture, by linking the DG inverters to the BSS inverter (as the Master) via low bandwidth communication. Alternatively, in agreement with the power sharing ideas presented in this paper, the desired adjustment of the DG inverters in the proposed microgrid may be achieved without telecommunication links, by using the current flow as the communication mechanism. In [34] the authors have explored the idea of Power Line Communication (PLC) via frequency signalling, which is illustrated in Fig. 11. A brief description is provided below.

A pre-determined frequency range, free of harmonics, is dedicated to PLC (e.g. 560 Hz to 640 Hz). Each DG inverter receives a PLC signal, mixed in the current stream, from the next DG inverter upstream. After estimating the PLC frequency, each DG inverter removes the previous PLC signal and re-injects its own PLC signal into the stream. This PLC signal is received by the next DG inverter downstream, etc.

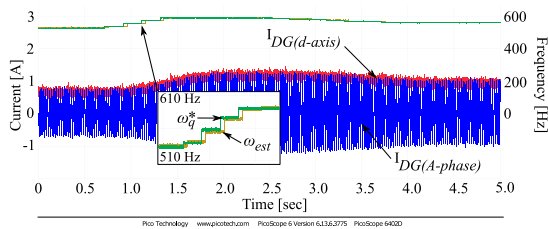


FIGURE 12. DG current adjustment by using PLC (experiment).

The frequency of the received PLC has the meaning of per unit loading of each DG inverter (e.g. 560 Hz means zero, 640 Hz means 100% of the rated power). This information, received by DG_j from its upstream neighbour DG_{j+1} , is compared to the DG_j own per unit loading. The difference is fed to a slow integral-type controller that adjusts the share D_j until, in steady state, per loading is equiaized between the neighbouring DGs. This ultimately leads to equitable loading of all working DGs, in proportion to the adjusted capacity.

To continue having identical dynamics, the steady-state per unit loading adjustments of DGs is accompanied by the corresponding relative change of their control gains. Due to bandwidth separation, the slow-acting PLC-based does not affect the main current sharing mechanism [34].

Fig. 11 illustrates how the described principle leads to adjustment of the currents i_{S1} , i_{S2} and i_{S4} , following a sudden drop in current i_{S3} . The corresponding experimental results for the leftmost, DG_4 , inverter appear in Fig. 12.

VI. CONCLUSION

In this paper, a novel concept of decentralized AC microgrid has been proposed, with load sharing based on measurement of downstream current. The proposed microgrid also provides automatic load sharing between the distributed generators, in proportion to their capacities. Unlike droop control, it needs no secondary control for the setpoint restoration. The proposed microgrid offers simple and stable dynamics as with Master-Slave control. Moreover, this is achieved without using high-bandwidth communication at the power sharing level.

Detailed simulations of the AC microgrid have demonstrated its effective load sharing capability. A stability study performed in the paper has shown that the proposed AC microgrid exhibits a stable first order dynamics when loaded by either CCL, CIL or CPL. An extension of the proposed strategy, allowing for load sharing adjustment via PLC, has also been explored.

Experimental results, included in the paper, closely agree with the simulations. They validate the proposed load sharing concept, stability in the presence of different load types, and effectiveness of the proposed fault tolerance strategy.

REFERENCES

[1] Y. Yang, Y. Qin, S. Tan, and S. Y. R. Hui, "Reducing distribution power loss of islanded AC microgrids using distributed electric springs with predictive control," *IEEE Trans. Ind. Electron.*, vol. 67, no. 10, pp. 9001–9011, Oct. 2020.

[2] E. Espina, J. Llanos, C. Burgos-Mellado, R. Cárdenas-Dobson, M. Martínez-Gómez, and D. Saez, "Distributed control strategies for microgrids: An overview," *IEEE Access*, vol. 8, pp. 193412–193448, 2020.

[3] J. Rocabert, A. Luna, F. Blaabjerg, and P. Rodriguez, "Control of power converters in AC microgrids," *IEEE Trans. Power Electron.*, vol. 27, no. 11, pp. 4734–4749, Nov. 2012.

[4] *Guide for Smart Grid Interoperability of Energy Technology and Information Technology Operation with the Electric Power System (EPS), End-Use Applications, and Loads*, IEEE 2030-2011 2011.

[5] E. Bullich-Massague, M. Aragues-Penalba, E. Prieto-Araujo, A. Sumper, and R. Caire, "Optimal feeder flow control for grid connected microgrids," *Int. J. Elect. Power Energy Syst.*, vol. 112, pp. 144–155, 2019.

[6] S.-J. Ahn, J.-W. Park, I.-Y. Chung, S.-I. Moon, S.-H. Kang, and S.-R. Nam, "Power-sharing method of multiple distributed generators considering control modes and configurations of a microgrid," *IEEE Trans. Power Del.*, vol. 25, no. 3, pp. 2007–2016, Jul. 2010.

[7] D. Pattabiraman, R. H. Lasseter, and T. M. Jahns, "Feeder flow control method with improved power sharing performance in microgrids," in *Proc. IEEE Power Energy Soc. Gen. Meeting*, 2017, pp. 1–5.

[8] D. I. Brandao, T. Caldognetto, F. P. Marafao, M. G. Simoes, J. A. Pomilio, and P. Tenti, "Centralized control of distributed single-phase inverters arbitrarily connected to three-phase four-wire microgrids," *IEEE Trans. Smart Grid*, vol. 8, no. 1, pp. 437–446, Jan. 2017.

[9] H. Han, X. Hou, J. Yang, J. Wu, M. Su, and J. M. Guerrero, "Review of power sharing control strategies for islanding operation of AC microgrids," *IEEE Trans. Smart Grid*, vol. 7, no. 1, pp. 200–215, Jan. 2016.

[10] R. R. Kolluri, I. Mareels, T. Alpcan, M. Brazil, J. Hoog, and D. A. Thomas, "Power sharing in angle droop controlled microgrids," *IEEE Trans. Power Syst.*, vol. 32, no. 6, pp. 4743–4751, Nov. 2017.

[11] M. S. Golsorkhi, Q. Shafiee, D. D.-C. Lu, and J. M. Guerrero, "Distributed control of low-voltage resistive AC microgrids," *IEEE Trans. Energy Convers.*, vol. 34, no. 2, pp. 573–584, Jun. 2019.

[12] A. Trivedi and M. Singh, "Adaptive droop control for AC microgrid with small mesh network," *IEEE Trans. Ind. Electron.*, vol. 65, no. 6, pp. 4781–4789, Jun. 2018.

[13] J. Liu, Y. Miura, and T. Ise, "Cost-function-based microgrid decentralized control of unbalance and harmonics for simultaneous bus voltage compensation and current sharing," *IEEE Trans. Power Electron.*, vol. 34, no. 8, pp. 7397–7410, Aug. 2019.

[14] J. Lu, M. Zhao, S. Golestan, T. Dragicevic, X. Pan, and J. M. Guerrero, "Distributed event-triggered control for reactive, unbalanced and harmonic power sharing in islanded AC microgrids," *IEEE Trans. Ind. Electron.*, vol. 69, no. 2, pp. 1548–1560, Feb. 2022.

[15] A. S. Vijay, N. Parth, S. Doolla, and M. C. Chandorkar, "An adaptive virtual impedance control for improving power sharing among inverters in islanded AC microgrids," *IEEE Trans. Smart Grid*, vol. 12, no. 4, pp. 2991–3003, Jul. 2021.

[16] A. Das, A. Shukla, A. B. Shyam, S. Anand, J. M. Guerrero, and S. R. Sahoo, "A distributed-controlled harmonic virtual impedance loop for AC microgrids," *IEEE Trans. Ind. Electron.*, vol. 68, no. 5, pp. 3949–3961, May 2021.

[17] Z. Peng *et al.*, "Droop control strategy incorporating coupling compensation and virtual impedance for microgrid application," *IEEE Trans. Energy Convers.*, vol. 34, no. 1, pp. 277–291, Mar. 2019.

[18] R. Zhang and B. Hredzak, "Nonlinear sliding mode and distributed control of battery energy storage and photovoltaic systems in AC microgrids with communication delays," *IEEE Trans. Ind. Informat.*, vol. 15, no. 9, pp. 5149–5160, Sep. 2019.

[19] G. Lou, W. Gu, Y. Xu, W. Jin, and X. Du, "Stability robustness for secondary voltage control in autonomous microgrids with consideration of communication delays," *IEEE Trans. Power Syst.*, vol. 33, no. 4, pp. 4164–4178, Jul. 2018.

[20] J. Lai and X. Lu, "Nonlinear mean-square power sharing control for AC microgrids under distributed event detection," *IEEE Trans. Ind. Informat.*, vol. 17, no. 1, pp. 219–229, Jan. 2021.

[21] Y. Chen, C. L. D. Q. Z. Li, Z. Wang, and J. Zhang, "Distributed event-triggered secondary control for islanded microgrids with proper trigger condition checking period," *IEEE Trans. Smart Grid*, vol. 13, no. 2, pp. 837–848, Mar. 2022.

[22] E. Hossain, R. Perez, A. Nasiri, and S. Padmanaban, "A comprehensive review on constant power loads compensation techniques," *IEEE Access*, vol. 6, pp. 33285–33305, 2018.

- [23] J. Chen and J. Chen, "Stability analysis and parameters optimization of islanded microgrid with ideal and dynamic constant power loads," *IEEE Trans. Ind. Electron.*, vol. 65, no. 4, pp. 3263–3274, Apr. 2018.
- [24] D. K. Dheer, A. S. Vijay, O. V. Kulkarni, and S. Doolla, "Improvement of stability margin of droop-based islanded microgrids by cascading of lead compensators," *IEEE Trans. Ind. Appl.*, vol. 55, no. 3, pp. 3241–3251, May/Jun. 2019.
- [25] A. Mortezaei, M. G. Simoes, M. Savaghebi, J. M. Guerrero, and A. Al-Durra, "Cooperative control of multi-master-slave islanded microgrid with power quality enhancement based on conservative power theory," *IEEE Trans. Smart Grid*, vol. 9, no. 4, pp. 2964–2975, Jul. 2018.
- [26] M. B. Delghavi and A. Yazdani, "Sliding-mode control of AC voltages and currents of dispatchable distributed energy resources in master-slave-organized inverter-based microgrids," *IEEE Trans. Smart Grid*, vol. 10, no. 1, pp. 980–991, Jan. 2019.
- [27] D. Kalke, H. M. Suryawanshi, G. G. Talapur, R. Deshmukh, and P. Nachankar, "Modified droop and master-slave control for load sharing in multiple standalone AC microgrids," in *Proc. 45th Annu. Conf. IEEE Ind. Electron. Soc.*, 2019, pp. 1862–1867.
- [28] J. Lai, X. Lu, X. Yu, W. Yao, J. Wen, and S. Cheng, "Distributed multi-DER cooperative control for master-slave-organized microgrid networks with limited communication bandwidth," *IEEE Trans. Ind. Informat.*, vol. 15, no. 6, pp. 3443–3456, Jun. 2019.
- [29] M. Ramezani, S. Li, and Y. Sun, "Combining droop and direct current vector control for control of parallel inverters in microgrid," *IET Renewable Power Gener.*, vol. 11, no. 1, pp. 107–114, 2017.
- [30] G. Mirzaeva, C. D. Townsend, D. Semenov, and G. C. Goodwin, "Decentralised control of parallel inverters in an AC microgrid using downstream current as an implicit communication method," in *Proc. IEEE Southern Power Electron. Conf.*, 2017, pp. 1–6.
- [31] P. Vas, *Sensorless Vector and Direct Torque Control*. London, UK: Oxford Univ. Press, 1998.
- [32] R. S. Pena, R. J. Cardenas, G. M. Asher, and J. C. Clare, "Vector controlled induction machines for stand-alone wind energy applications," in *Proc. 35th Annu. Meeting IEEE Ind. Appl. Soc.*, vol. 3, 2000, pp. 1409–1415.
- [33] D. Semenov, G. Mirzaeva, and G. C. Goodwin, "Inverter control and implementation options for a novel AC microgrid," in *Proc. IEEE Symp. Power Electron. Elect. Drives Automat. Motion*, 2018, pp. 722–727.
- [34] D. Miller, G. Mirzaeva, C. D. Townsend, and G. C. Goodwin, "The use of power line communication in standalone microgrids," *IEEE Trans. Ind. Appl.*, vol. 57, no. 3, pp. 3029–3037, May/Jun. 2021.



DMITRY MILLER received the B.S. degree in power engineering from Ural Federal University, Yekaterinburg, Russia, in 2014, the M.S. degree in electrical engineering from the Harbin Institute of Technology, Harbin, China, in 2016, and the Ph.D. degree in electrical engineering from the University of Newcastle, Callaghan, NSW, Australia, in 2021. He currently is currently an Engineer with Ampcontrol CSM, Australia. His research interests include power electronics, electric drives, microgrids, and electric transportation.



GALINA MIRZAEVA (Senior Member, IEEE) received the B.Eng. degree in electronic engineering and the Ph.D. degree in electrical engineering from South Urals State University, Chelyabinsk, Russia, in 1990 and in 1997, respectively.

From 2004 to 2010, she was a Senior Researcher with CRC-Mining, Australia. Since 2010, she has been with the School of Electrical Engineering and Computing, University of Newcastle, Callaghan, NSW, Australia, first as Senior Lecturer, and has been an Associate Professor since 2017. Her research interests include electric machines and drives, power electronics, and renewable energy applications. From 2009 to 2011, was the Chair of the IEEE IAS Mining Industry Committee, where he has also been the Chair since 2020.



CHRISTOPHER DAVID TOWNSEND (Member, IEEE) received the B.E. and Ph.D. degrees in electrical engineering from the University of Newcastle, Callaghan, NSW, Australia, in 2009 and 2013, respectively. He held research positions with ABB Corporate Research, Sweden, the University of New South Wales, Sydney NSW, Australia, University of Newcastle, and Nanyang Technological University, Singapore. In 2019, he joined the Department of Electrical, Electronic and Computer Engineering, University of Western Australia, Perth, WA, Australia, as a Senior Lecturer. His research interests

include topologies and modulation strategies for multilevel converters applied in power systems, renewable energy integration, and electric vehicle applications.



GRAHAM C. GOODWIN (Life Fellow, IEEE) received the B.Sc. degree in physics, the B.E. (with Hons.) degree in electrical engineering, and the Ph.D. degree in electrical engineering from the University of New South Wales, Sydney NSW, Australia, in 1965, 1967, and 1971, respectively. He is currently an Honorary Fellow of the Institute of Engineers, Australia, a Fellow of the International Federation of Automatic Control, a Fellow of the Australian Academy of Science, a Fellow of the Royal Society, London, and a Foreign Member

of the Royal Swedish Academy of Sciences. His current research interests include control applications to power electronics, industrial automation, and biomedical fields.